400-Mev Neutron-Proton Scattering*

A. J. HARTZLER AND R. T. SIEGEL
Carnegie Institute of Technology, Pittsburgh, Pennsylvania
(Received March 5, 1954)

The angular distribution of neutron-proton scattering has been measured at a neutron energy of 400 Mev, with energy resolution of 7 percent. The counter telescope used to detect recoil protons was calibrated in an auxiliary experiment which also gave information about proton-proton scattering at several energies in the 400-Mev region.

The n-p cross section has the same general characteristics observed at lower energies, with a minimum at about 100° (c.m. neutron scattering angle) and a large exchange peak at 180°. The p-p results indicate an isotropic cross section below 400 Mev, and a rise at small angles at 428 Mev.

I. INTRODUCTION

WITH the availability of large synchrocyclotrons it has been possible to extend neutron-proton scattering experiments far beyond the "classical" region of <10 Mev to energies as high as 300 Mev.[1–8] Although these high-energy experiments are not completely understood theoretically, certain experimental features of the angular distributions are clear. First, a deep minimum occurs in the center-of-mass (c.m.) cross section at about 90°, with a large peak at 180° (neutron scattering angle) caused by exchange scattering. Second, recent cloud-chamber experiments by Powell[9] and coworkers at Berkeley have given strong support to the Serber force (half-ordinary, half-exchange) with a 90-Mev distribution which is symmetric about the 90° minimum. In contrast, DePangher[8] finds that at 300 Mev the small-angle scattering is lower by a factor of two or three than the 180° exchange scattering. Further, high-energy measurements show that the ratio $4(d\sigma/d\Omega)_{n-p}^{90°}/(d\sigma/d\Omega)_{p-p}^{90°}$ is approaching unity, the lower limit permitted by the charge-independence hypothesis.

It is naturally of interest to study the n-p interaction at even higher energies. In the experiment reported here, the neutron beam of the 440-Mev Carnegie cyclotron was used to measure the angular distribution of n-p scattering at a mean incident energy of 400 Mev. As in all such experiments to date, the recoil protons have been detected and the angular distribution of scattered neutrons deduced from the kinematic relations summarized below. The symbols are mostly those used by Hadley *et al.*[1]

$m_n=m_p=1$;
E_n = incident neutron lab KE $=\gamma-1$, $\gamma=1/(1-\beta^2)^{\frac{1}{2}}$;
E_p = recoil proton lab KE;
Φ, φ = recoil proton lab and c.m. angle, respectively;
Θ, θ = scattered neutron lab and c.m. angle, respectively;

$$\tan\Phi=[2/(\gamma+1)]^{\frac{1}{2}}\cot(\theta/2);$$

$$E_p=\tfrac{1}{2}E_n(1+\cos\varphi)=\tfrac{1}{2}E_n(1-\cos\theta);$$

$$J=\frac{d(\cos\Phi)}{d(\cos\theta)}=\frac{1}{8\cos\Phi}[(\gamma+1)-(\gamma-1)\cos^2\Phi]\frac{1}{\gamma+1}.$$

Primarily we are interested in the *variation* of recoil proton counting rate with laboratory angle, which yields *relative* differential cross sections. When these have been obtained for all angles, *absolute* cross sections can be calculated by normalization of the integrated relative cross section to the total n-p cross section as measured by a transmission experiment.[10]

II. GENERAL DESCRIPTION OF THE EXPERIMENT

The experimental arrangement is shown schematically in Fig. 1. The neutron beam emerged from the

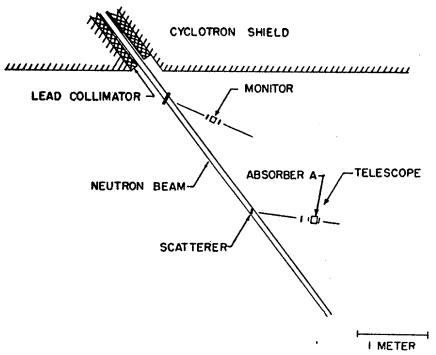

FIG. 1. Experimental arrangement.

* Work supported in part by the U. S. Atomic Energy Commission.

[1] Hadley, Kelly, Leith, Segrè, Wiegand, and York, Phys. Rev. **75**, 351 (1949).
[2] Brueckner, Hartsough, Hayward, and Powell, Phys. Rev. **75**, 555 (1949).
[3] Kelly, Leith, Segrè, and Wiegand, Phys. Rev. **79**, 96 (1950); **83**, 923 (1951).
[4] R. H. Fox, University of California Radiation Laboratory Report UCRL-867, 1950 (unpublished).
[5] Guernsey, Mott, and Nelson, Phys. Rev. **88**, 15 (1952).
[6] Randle, Taylor, and Wood, Proc. Roy. Soc. (London) **213**, 392 (1952).
[7] Selove, Strauch, and Titus, Phys. Rev. **92**, 724 (1953).
[8] J. DePangher, Phys. Rev. **92**, 1084 (1953), University of California Radiation Laboratory Report UCRL-2153 (unpublished).
[9] Reported by Professor Powell at the Annual Meeting of the American Physical Society in New York, January 26–28, 1954 [Bull. Am. Phys. Soc. **29**, No. 1, 49 (1954)].
[10] V. A. Nedzel, Phys. Rev. **91**, 440 (1953) reports a total n-p cross section of $(33.6\pm1)\times10^{-27}$ cm² at 400 Mev.

shielding wall through a three-inch diameter hole and was monitored by a scintillation telescope counting recoil particles from a one-inch thick polyethylene plate. This monitor telescope was fixed at approximately 30° to the beam, and a copper absorber between its two counters insured that only the neutrons above 350 Mev were monitored.

The beam then impinged upon the scattering apparatus, in which recoil particles from polyethylene, carbon, and with no scatterer in place were counted as a function of angle by a three-crystal scintillation telescope. A copper absorber (A) between the last two counters was adjusted in thickness at each angle to make the apparatus insensitive to protons produced in n-p collisions of incident energy less than 365 Mev. A wide range of absorber thicknesses (0.03 in. to 4.45 in.) was necessary for this purpose in the angular region studied. As a result of variations in the loss of protons by nuclear absorption and scattering, there was a large change in telescope efficiency with angle. In order to avoid uncertain calculations of these effects, the efficiency was measured experimentally, as described in Sec. VI.

To obtain the n-p angular distribution, the number of coincidence counts per unit monitor (=10 000 counts) at each angle was measured for each type of scatterer, and the net hydrogen effect was calculated. The CH_2 and carbon scatterers were of approximately equal stopping power; their weights were such that the hydrogen effect was given by

$$R_H=(R_{CH_2}-R_{B1})-0.73(R_C-R_{B1})$$
$$=R_{CH_2}-0.73R_C-0.27R_{B1},$$

where R_{B1} is the "no scatterer" rate.

The n-p data gathered during ten cyclotron runs were normalized to the results of run No. 5 (September 17, 1953), which included the most comprehensive set of measurements. The normalization procedure was as follows: let R_C^1 and R_C^2 be the counting rates obtained from carbon (with background subtracted) at a certain angle on days 1 and 2, respectively. The ratio R_C^1/R_C^2 indicates the change in experimental (i.e., monitoring) conditions between the two days and is therefore the normalizing factor to be used in reducing the data to a single scale. The ratio $R_{CH_2}^1/R_{CH_2}^2$ should be equal to this factor, as should all similar ratios calculated for the angles common to the two runs. By combining all the available data from each pair of runs it was possible to obtain the normalization factors to an accuracy much greater than that of any individual hydrogen effect measurement. The accuracy of each normalizing factor was then calculated both from statistical considerations and from the spread in individual values obtained as above, the two methods yielding the same results.

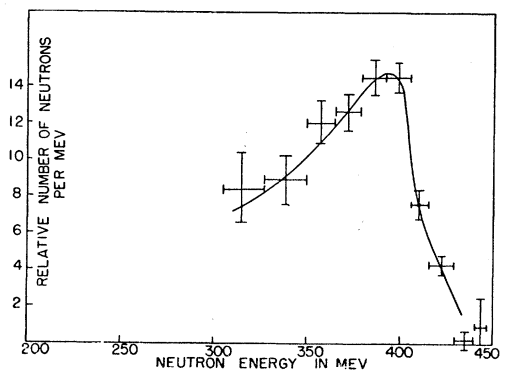

FIG. 2. Differential range curve of recoil protons at 23.0° to the neutron beam. The abscissae have been altered from inches of copper to Mev to facilitate comparison with Fig. 3.

III. THE NEUTRON BEAM

The neutrons were produced by bombardment of a 1-in. thick beryllium target in the cyclotron at a radius corresponding to 427-Mev proton energy. Neutrons emitted in the forward direction were collimated by seven feet of lead spaced at various depths in a total thickness of thirteen feet of magnetite concrete. The defining aperture for this beam was a 2-in. diameter hole at 27 feet from the internal target.

The spectrum of the neutrons was deduced from a differential range curve (Fig. 2) of protons ejected at 23° to the beam from an effective hydrogen target. Since the efficiency of the telescope varies with absorber thickness, this range curve does not give the true neutron spectrum directly. The telescope was therefore calibrated (with the same technique described in Sec. VI) at the fixed 23° angle for changes in efficiency introduced by the absorbers, and this effect unfolded from the range curve to give the spectrum of Fig. 3. The errors shown in this figure were obtained by considering the extreme spectra compatible with the errors in Fig. 2. Although the uncertainties in the spectrum of Fig. 3 are not small, their effect on the accuracy of the entire experiment is unimportant. (See Sec. VI.)

Exposures of x-ray film were made at frequent intervals during the experiment for alignment purposes, as well as to study the uniformity of the beam. The radiographs at the position of the scatterer showed a circular spot about three inches in diameter, the top and bottom being somewhat diffuse because the source of neutrons is a vertical line. Because the scatterers were smaller than the beam, it was desirable for the neutron intensity to be uniform over a large part of the beam area. Many x-ray photographs indicated that this was in fact the case. As another test for uniformity, one entire cyclotron run was made with scatterers and table shifted $\frac{1}{4}$ in. sideways relative to the beam center. Results consistent with the other runs were obtained. Finally, the counter telescope was fixed at 18° to the beam and the thinnest carbon scatterer rotated until it was parallel to the beam direction. No effect on the

counting rate (within ~1 percent) was observed. On the basis of these tests it was concluded that the beam was sufficiently uniform for our purposes.

Before the experiment was begun the beam was investigated for charged particle contamination. As a test a magnetic sweeping field was used to remove any such impurities; the observed change in rate in a single scintillation counter placed in the beam corresponded to less than 0.1 percent charged particles. Nuclear plates were also exposed in and near the beam, the number of tracks counted again indicating about 0.1 percent contamination.

Under normal cyclotron conditions the intensity of neutrons above 365 Mev was about 2×10^5 cm^{-2} sec^{-1}.

IV. GEOMETRY AND SCATTERERS

The angular aperture of the recoil telescope was defined by the second counter, a stilbene crystal 3 cm wide ×6 cm high. This was located 80 cm from the scatterer when angles greater than 9° were being investigated, and was moved out to twice that distance for the smaller angles. (See Table I.) At 2.3° it was necessary to move it to 210 cm in order to keep the first counter well away from the direct neutron beam, but at zero degrees a distance of 80 cm was again chosen as a compromise between large scattered flux and good angular resolution. At the 80-cm distance the resolution curve for nonzero angles should be trapezoidal with a full width at half-maximum of 3.2°. Hence measurements at five degree intervals effectively do not overlap.

TABLE I. Geometry and scatterers.

Geometry	Distance of counter No. 2 from scatterer center (cm)	Solid angle subtended by counter No. 2 (sterad)
α	80	2.81×10^{-3}
β	160	7.03×10^{-4}
γ	210	4.08×10^{-4}
Scatterer set	**Weight of CH_2 scatterer (g)**	**Weight of C scatterer (g)**
I	11.43	13.44
II	22.92	26.88
III	42.50	49.83

The scatterers were accurately machined and weighed plates of polyethylene and carbon 4.45 cm square. Three different sets of matched scatterers with surface densities in the ratios 1.00:2.00:3.72 were used (see Table I), the thinnest set being employed primarily at angles above 57.6° where the energy of the recoil protons is lowest.

Several tests confirmed that the geometrical properties of the apparatus were as expected. It was observed that the counting rates from either carbon or polyethylene scatterers (after subtraction of background) were unchanged on displacement of the first counter along the telescope axis, and also that these rates varied inversely as the square of the "defining" distance to counter No. 2. In addition, different sets of scatterers were used at 57.6°, 9.1°, and 4.6° to verify that at each of these angles a proportionality existed between surface density and scattered flux.

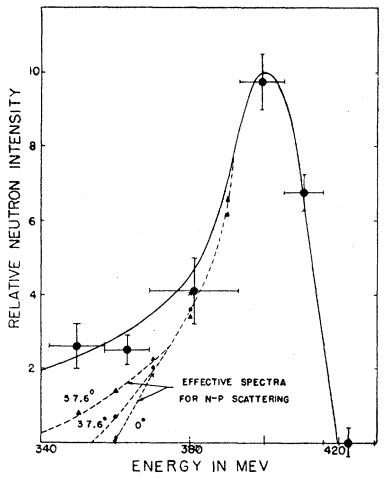

FIG. 3. Corrected neutron spectrum from 427-Mev protons on Be. The dotted curves show the effect of absorber A at the scattering angles indicated.

V. APPARATUS AND PERFORMANCE

The three scintillation counters each consisted of a stilbene crystal mounted on a Lucite light-pipe and viewed by an RCA 5819 photomultiplier. The first two crystals, $4\times6\times\frac{1}{2}$ cm and $3\times6\times\frac{1}{2}$ cm, respectively, were viewed from the sides and covered with 0.001-in. aluminum foil to shield them from external light. The third crystal, $5\times10\times\frac{1}{2}$ cm, was viewed normal to its large surface, and was always positioned 15.0 cm behind the second counter. Absorber A (Fig. 1) was 7.5 cm wide×12.5 cm high. At each angle its thickness was equal to the range of a proton ejected by a 365-Mev neutron from the center of the scatterer and proceeding along the axis of the telescope. Energy losses in the crystals, scatterer, etc., were computed from the tables of Aron,[11] and the absorber thickness adjusted accordingly.

Anode pulses from the three multipliers were fed into cathode followers and then through fifty-foot cables to the counting area. There the pulses were amplified with distributed amplifiers and passed through inverter-limiters, finally entering a diode coincidence circuit of standard design. Clipping stubs at the coincidence chassis provided a resolving time of about 10^{-8} second. Both triple coincidences and double coincidences between counters No. 1 and No. 2 were then amplified and scaled.

[11] W. A. Aron, University of California Radiation Laboratory Report UCRL-1325, 1951 (unpublished).

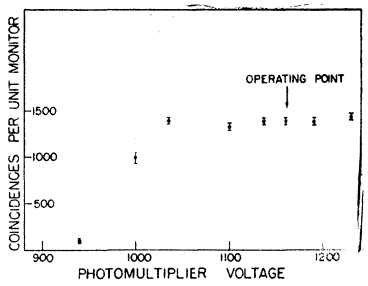

FIG. 4. High voltage plateau of triple coincidence circuit taken on October 14, 1953.

At the beginning of each run tests on the performance of the apparatus were carried out as follows. A discriminator plateau was taken with the linear amplifier following each coincidence circuit, showing plateaus about thirty volts wide. The master high-voltage control on all three multipliers was then varied to measure a plateau as shown in Fig. 4. Such plateaus were about 150 volts wide, while an electrostatic voltmeter on each supply indicated drifts of less than twenty volts during the course of any run.

Delay curves were found to be flat-topped in the neighborhood of coincidence and also near 5×10^{-8} sec (corresponding to one cyclotron radio-frequency cycle). The number of accidental coincidences was measured by delaying each of the counters in turn by one rf cycle; as expected, most accidentals were caused by a true double coincidence between counters No. 1 and No. 2 occurring simultaneously with a random single count in No. 3. Except during the measurement of proton recoils at 0°, these accidental coincidences were always less than $\frac{1}{2}$ percent of the counts observed from any scatterer.

Detection of scattered protons at 0° to the beam involves special difficulties, because the counter telescope must be placed in the direct neutron flux. At full beam strength this causes overloading of the multipliers as well as impossibly high accidental rates, so a cyclotron level about 5 percent of normal was used during the 0° measurements. With this intensity accidental rates averaged about 20 percent of the counting rates. In order to avoid errors in the measurement of accidentals during these 0° runs, only data taken with constant monitor rate (±4 percent) were accepted.

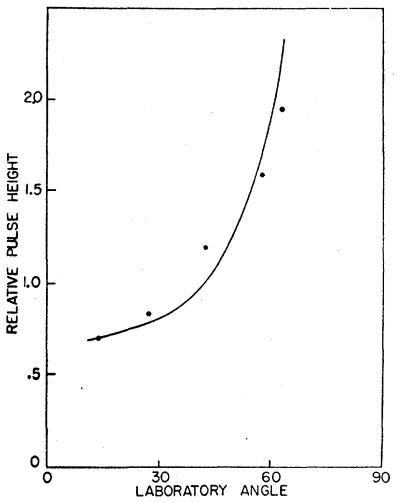

FIG. 5. Pulse height in counter No. 1 *vs* telescope angle. Experimental points are normalized at 13.8° to curve (calculated for 400-Mev *n-p* recoil protons).

For the calibration experiment, the external proton beam from the cyclotron was scattered with the same apparatus used with neutrons. The greater intensity of protons made possible more detailed checks of the equipment than were possible with the neutron beam. The accidental coincidences at small angles to the proton beam were often several percent of the total counting rates, and a much sharper peaking of the accidental rates about one rf cycle of delay was observed. With the proton beam, delay curves were followed out to four rf cycles with no loss of accidental rates, indicating that attenuation in the delay cables introduced no error.

The counting rate per unit monitor count was measured with the proton beam over a wide range of beam intensities in order to detect possible dead-time losses in the counting system. Such losses were observed at high beam strengths, and corrections to the data were made accordingly. With the neutron beam losses were never a problem.

One test remains to be described. If the recoil particles detected by our telescope are really protons from 400-Mev *n-p* collisions, their energies and thus dE/dx in the stilbene crystals are easily calculated. In order to leave no doubt about the nature of the particles giving triple coincidences, a study was made of the pulse amplitudes from the first counter of the telescope as a function of angle. The pulses were analyzed by a twenty-four-channel pulse-height selector[12] which was triggered by the triple coincidences, and the data obtained for each scatterer processed in the usual way to find the location of the average pulse height from an effective hydrogen scatterer. These average amplitudes, normalized at 13.8° to the curve calculated for recoil protons from *n-p* collisions, are shown in Fig. 5. Considering the 10-percent resolution of the crystal, there is excellent agreement between the points and the curve.

The pulse-height distributions from carbon are somewhat broader than those from hydrogen, but have similar average amplitudes. Both characteristics indicate a quasi *n-p* scattering as the source of most particles observed from carbon.

VI. CALIBRATION OF THE APPARATUS

As pointed out in Sec. II, the efficiency of the counter telescope may be expected to vary considerably with

[12] This pulse-height analyzer was lent to us by DeBenedetti, Stearns, and Stearns of this laboratory.

angle. One way to measure this efficiency is to place the counters directly in a proton beam of variable energy and observe the ratio of triple coincidences to double coincidences between the first two counters. This gives the transmission of absorber A, i.e., the efficiency of the telescope. However, the scattered protons detected in the n-p experiment do not strike the telescope as a parallel, monoenergetic beam, but as a spreading flux from a small source (the scatterer), with energy varying over the aperture of the counters.

The high-intensity ($\sim 4\times 10^6$ cm^{-2} sec^{-1}) external proton beam of the Carnegie cyclotron provided a way of calibrating the counter telescope which automatically compensated for these effects. By scattering this beam (enlarged so that it was 2.5 in.$\times$2.5 in. square) from hydrogen in the same geometry used with the neutron beam, a scattered flux which had the same

TABLE II. Net counter telescope efficiency *vs* angle. Errors average ±3 percent of the values given.

Φ	Absorber A (inches of Cu)	Net efficiency
0	4.45	0.35
2.3	4.43	0.35
4.6	4.39	0.36
6.8	4.33	0.36
9.1	4.23	0.37
13.8	4.00	0.38
18.5	3.65	0.40
23.0	3.23	0.41
27.8	2.77	0.44
32.6	2.28	0.48
37.4	1.80	0.50
42.4	1.34	0.53
47.2	0.93	0.56
52.4	0.58	0.60
57.6	0.33	0.56
60.7	0.24	0.58
63.2	0.14	0.55
65.5	0.07	0.60
68.2	0.03	0.41

energy-angle distribution as the recoil protons from n-p collisions was obtained. The ratio triples/doubles then gave the telescope efficiency under the proper experimental conditions.

After passing through the monitor scatterer, the protons had an energy of 428 Mev as measured by a Bragg curve. They were degraded with polyethylene absorbers to 410, 395, 380, 365, 357 Mev successively, thus spanning the useful energy region of the neutron spectrum. At each proton energy (including 428 Mev), double and triple coincidences were measured as a function of angle from 68.2° to 18.5°, background usually being prohibitive at smaller angles. However, at 0° the efficiency could be measured by direct transmission, and values between 18.5° and 0° obtained by interpolation.

Figure 6 is a sample plot of efficiency *vs* energy at a fixed angle. Such data correspond to a transmission *vs* energy measurement in a particular geometry, so a

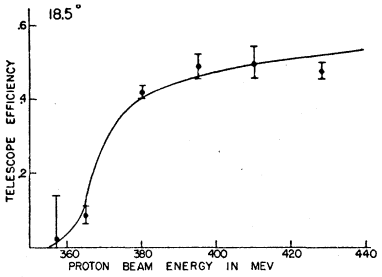

FIG. 6. Telescope efficiency at 18.5° as a function of incident proton energy.

smooth curve may be drawn through the points. Ordinates taken from this and similar graphs at other angles were folded into the neutron spectrum to obtain net efficiencies shown in Fig. 7 and Table II. The average error of about 3 percent quoted for these efficiencies was derived from (1) random errors assigned to the efficiencies on the basis of fluctuation of the experimental points about a smooth curve, and (2) variation in the net efficiencies introduced by using extreme shapes of the neutron spectrum allowed by the data of Fig. 3. The former errors are closely related to actual counting statistics, but are often smaller because of the regular and predictable variation with energy of the efficiency at any one angle. The latter type of error is much less important because of the sharp peak in the spectrum.

Complete proton range curves were also taken at various incident energies. Since the telescope is a "poor" geometry device for this purpose, the initial slopes of these curves should give nuclear cross sections for protons in copper. However, fragments from nuclear collisions made by the protons will penetrate a small thickness of Cu and lower the apparent cross section deduced from the beginning of the range curve. These fragments also cause a hump in the Bragg curves for 428-Mev protons at small copper thicknesses. Therefore, the slope of the range curves between 0.5 in. and 1.5 in. was chosen as a measure of the nuclear absorption

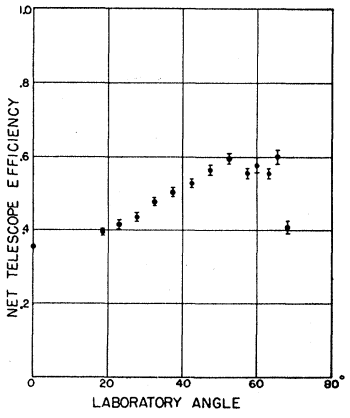

FIG. 7. Net telescope efficiency *vs* angle.

cross section. At 400 Mev this yields a σ_a of 0.50 barn ± 10 percent (minimum half-angle subtended $= 18°$).

Finally, we note from the effective neutron spectra plotted in Fig. 3 that the maximum of intensity always lies at 400 ± 5 Mev and that the full width at half-maximum is ~ 30 Mev.

VII. PROTON-PROTON SCATTERING

The scattering method of calibration described above requires correction for charged particles which are produced in p-p collisions and detected along with elastically scattered protons. The principal contaminants are mesons from $p+p \rightarrow \pi^+ + d$. a process which has been investigated in this energy region.[13] The evidence indicates a c.m. angular distribution for the π mesons of the form $(0.2+\cos^2\theta)$, and a total cross section rising linearly from 0.6 mb at 365 Mev to 1.3 mb at 430 Mev. Corrections for these mesons have been applied to both the double and triple coincidences, taking into account the attenuation in absorber A. These changes are generally less than 3 percent, so systematic errors resulting from uncertainty in the meson production cross section are probably less than 1 percent.

When the meson corrections have been made to the observed double coincidence rates, they should be proportional to the differential p-p scattering cross sections. After transformation to the center-of-mass system these data are summarized in Table III and Fig. 8. Since only one of the scattered protons is detected, cross sections are given for angles greater than 90°. The symmetry of the distributions about that point demonstrates that there is no systematic error introduced by large meson production at small angles, and also that there is no loss of protons in the scatterer or first crystal of the telescope at large angles.

Below 400 Mev these p-p data indicate no deviation from isotropy from 30°–90° within a few percent. At 410 Mev data are sparse, but at 428 a rise of about 10 percent at 40° (and 140°) is visible. This is in excellent agreement with the results of Mott, Sutton, *et al.* at 437 Mev and in disagreement with the results of Marshall *et al.* at 429 Mev.[14] It is worthy of note that in the experiments reported here n-p and p-p scattering have both been measured with the same apparatus and in identical geometries.

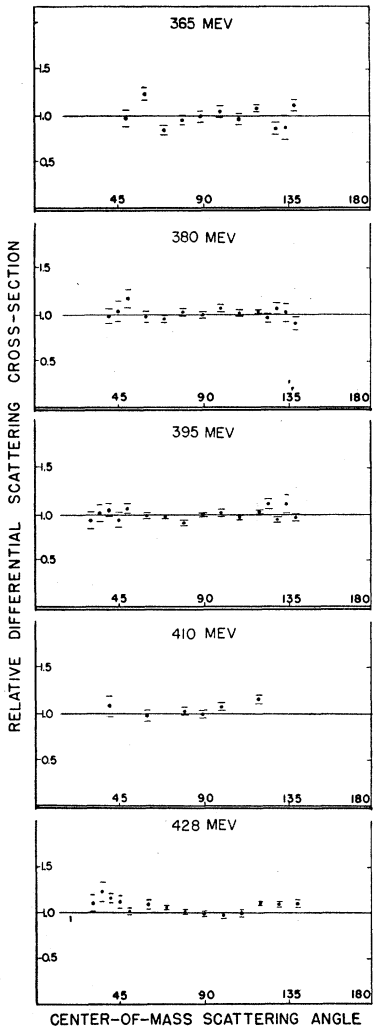

FIG. 8. Barycentric proton-proton scattering at five incident proton energies. Each angular distribution is normalized to $(d\sigma/d\Omega)_{p-p}{}^{90°} = 1.00$. Errors are standard deviations from counting statistics only.

[13] Fields, Fox, Kane, Stallwood, and Sutton, Bull. Am. Phys. Soc. **29**, No. 4, 50 (1954).

TABLE III. Barycentric proton-proton scattering cross sections, relative to $(d\sigma/d\Omega)_{p-p}{}^{90°} = 1.00$, at five incident energies. Errors are statistical standard deviations from counting only.

C.m. scattering angle	Incident proton energy in Mev 365	380	395	410	428
30			0.94 ±0.09		1.11 ±0.09
35			1.02 ±0.09		1.24 ±0.10
40		0.99 ±0.08	1.05 ±0.07	1.08 ±0.11	1.16 ±0.05
45		1.04 ±0.11	0.95 ±0.08		1.12 ±0.07
50	0.98 ±0.08	1.18 ±0.10	1.07 ±0.05		1.02 ±0.04
60	1.14 ±0.07	0.98 ±0.06	0.99 ±0.03	0.98 ±0.06	1.09 ±0.05
70	0.85 ±0.05	0.96 ±0.04	0.98 ±0.02		1.05 ±0.02
80	0.96 ±0.05	1.03 ±0.04	0.91 ±0.03	1.03 ±0.04	1.01 ±0.02
90	1.00 ±0.06	1.00 ±0.03	1.00 ±0.02	1.00 ±0.04	1.00 ±0.02
100	1.05 ±0.06	1.07 ±0.04	1.02 ±0.04	1.08 ±0.04	0.97 ±0.02
110	0.97 ±0.06	1.02 ±0.03	0.97 ±0.02		0.99 ±0.04
120	1.09 ±0.03	1.04 ±0.02	1.03 ±0.02	1.16 ±0.05	1.10 ±0.02
125		0.97 ±0.05	1.12 ±0.05		
130	0.87 ±0.07	1.07 ±0.06	0.95 ±0.03		1.09 ±0.03
135	0.88 ±0.13	1.03 ±0.09	1.12 ±0.10		
140	1.12 ±0.06	0.91 ±0.07	0.97 ±0.04		1.10 ±0.04

[14] Mott, Sutton, Fox, and Kane, Phys. Rev. **90**, 712 (1953); Marshall, Marshall, and Nedzel, Phys. Rev. **92**, 834 (1953). Some uncertainty remains in our p-p data because of the process $p+p \rightarrow \pi^+ + n + p$, which is negligible at lower energies but perhaps not at 428 Mev. A further correction equal to 40 percent of that already made for the two-body production would reduce the rise observed in the p-p cross section at 428 Mev to about 8 percent at 40°, barycentric angle. Results at and below 410 Mev would be unaffected within the experimental error.

TABLE IV. Laboratory n-p counts normalized to geometry α and scatterers II (see Table I). Errors are statistical standard deviations from counting only.

Φ \ No.	1 May 31	2 June 3	3 June 5	4 June 7	5 Sept. 17	6 Sept. 19	7 Sept. 30	8 October 2	9 October 14	10 October 16	Weighted average
0								3642±304		3992±435	3757±250
2.3					2538±327	2682±90					2672±76
4.6			2213±128		2224±78	2226±61	2155±84				2208±40
6.8			1685±81			1582±48	1682±61				1632±35
9.1	1528±63	1680±75	1491±58		1488±26	1427±35					1486±19
13.8					1166±26	1200±28	1166±42	1119±32	1202±26	1191±33	1177±13
18.5	878±33	971±46		949±34	902±20	924±22	885±25				911±11
23.0				701±25	763±33						707±16
27.8	555±25	664±30			567±21					503±23	543±14
32.6				432±16	406±28						425±16
37.4	386±16	434±20		412±33	357±27	396±28					386±12
42.4		397±15			392±19					402±16	397±10
47.2	455±20	473±26			451±20						453±14
52.4	474±22				534±25						500±17
57.6	439±20				464±23	410±36	465±22		429±27	424±19	445±9
60.7									432±35		432±35
63.2		493±33		394±48	496±32	532±27	453±42		484±33		489±14
65.5					524±42		429±36		498±34		480±22
68.2		203±33			338±30		323±36		314±29		289±14

VIII. n-p RESULTS AND ERRORS

In Table IV the n-p counts per unit monitor observed during each run are assembled along with their statistical counting errors, with weighted mean values given in the last column. The corresponding barycentric cross sections, normalized to unity at $\theta=90°$, are displayed in Table V and Fig. 9. The errors quoted for both the p-p and n-p cross sections (Tables III and V) are standard deviations computed for the following sources of uncertainty: (1) counting statistics in the n-p experiment; (2) random errors arising from counting statistics of the calibration (p-p) experiment; (3) uncertainties in the neutron spectrum; (4) uncertainties in measurement of dead-time losses, accidentals, etc. Not included are errors which may originate in plateau interpretation, mechanical alignment, scatterer impurities,[15] beam nonuniformity, and in the meson corrections to the p-p data. These may contribute an additional 3 percent error to be superimposed on the results given in Tables III and V.

We have not made the usual correction at small angles to compensate for change in slope of the cross section across the telescope aperture. Because of the resolution employed, these corrections are negligible except at 2.3° and 0°. With the data as presented in Table V, this correction would raise the cross section at 2.3° by

TABLE V. Barycentric neutron-proton scattering cross sections at 400 Mev relative to $(d\sigma/d\Omega)_{n-p}{}^{90°}=1.00$. Errors are combined statistical standard deviations from n-p counting, spectrum errors, and calibration errors.

Lab angle Φ	$J_{np}=\frac{d\cos\Phi}{d\cos\theta}$	c.m. angle θ	Relative $(d\sigma/d\Omega)_{n-p}$
0	0.207	180	8.74 ±0.59
2.3	0.207	175	6.20 ±0.22
4.6	0.208	170	5.14 ±0.18
6.8	0.209	165	3.77 ±0.14
9.1	0.211	160	3.40 ±0.09
13.8	0.218	150	2.70 ±0.07
18.5	0.227	140	2.08 ±0.06
23.0	0.239	130	1.62 ±0.06
27.8	0.255	120	1.26 ±0.05
32.6	0.276	110	0.972±0.044
37.4	0.302	100	0.923±0.036
42.4	0.336	90	1.00 ±0.04
47.2	0.377	80	1.20 ±0.04
52.4	0.433	70	1.44 ±0.06
57.6	0.508	60	1.61 ±0.05
60.2	0.558	55	1.66 ±0.15
63.2	0.623	50	2.19 ±0.08
65.5	0.686	45	2.17 ±0.13
68.2	0.773	40	2.16 ±0.13

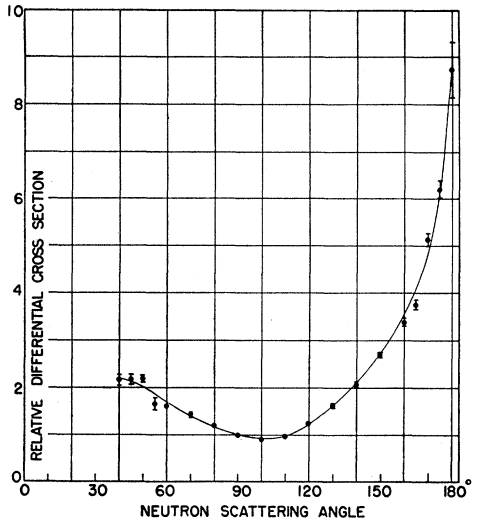

FIG. 9. Barycentric neutron-proton angular distribution at 400 Mev, normalized to $(d\sigma/d\Omega)_{n-p}{}^{90°}=1.00$. Errors are those given in Table V (see also Sec. VIII). (Near 90° the black dots are larger than the errors.)

[15] Chemical analysis of the polyethylene showed that its formula was $CH_{2.00}$ within about 0.5 percent error. The carbon contained less than 0.1 percent impurity.

2 percent, which is less than the experimental error at that point. At 0° a difficulty arises which is connected with the observed counts *vs* angle from carbon (Fig. 10). (Also shown in this figure are the counting rates, uncorrected for efficiency, from hydrogen and at small angles from an aluminum scatterer.) One sees that the cross sections for the production of high-energy protons by neutrons on carbon or aluminum are almost independent of angle between 5° and 30°. At higher angles interpretation is difficult because the telescope efficiency is known only for protons of selected energy, and not for recoils from quasi *n-p* collisions within nuclei. The tremendous peak in the carbon and aluminum counting rates below 5° is, we believe, a result of Rutherford scattering of the charged contaminants in the neutron beam. The sizes of the peaks and their relative magnitudes for aluminum and carbon are consistent with this hypothesis, but their persistence at 0° is not. It is difficult to imagine a nuclear effect which would produce as sharp a rise, and consequently the 0° measurement is open to suspicion. This is why no curvature corrections have been made at this angle.

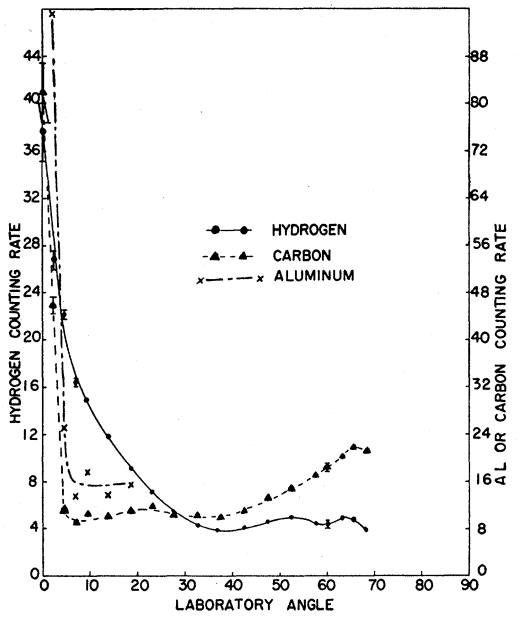

FIG. 10. Observed counts *vs* angle for H, C, and Al scatterers, normalized to equal numbers of scattering centers for the three elements.

IX. SUMMARY

The *n-p* angular distribution (Fig. 9) shows certain interesting features in contrast to lower energy results. The minimum in the curve has shifted to about 100°, and there is clearly a lack of symmetry about 90°. At small angles the cross section seems to be leveling off at a relative value of ~ 2.5. Extrapolation to this magnitude at 0° and integration to a total cross section of 34 mb[16] gives $(d\sigma/d\Omega)_{n-p}^{90°} = 1.5$ mb. This is large enough so that the condition imposed by charge independence (see Sec. I) is easily satisfied, since $(d\sigma/d\Omega)_{p-p}^{90°} = 3.5$ mb at 400 Mev. In fact, extrapolation of the *n-p* cross section to any reasonable value at 0° does not change this conclusion.

Further experiments at small neutron scattering angles would be of interest to ascertain whether the symmetry about 90° displayed by the scattering at lower energies is really destroyed at 300 Mev and above, as is suggested by these data and those of DePangher.[8] If so, the Serber potential cannot describe the *n-p* interaction at these energies.

The authors wish to thank Mr. Eugene Maier for help with the calculations and many members of the laboratory for helpful discussions.

[16] See reference 10. The meson production contributions to this total cross section arise mostly from $n+p \rightarrow \pi^0+d$, which according to charge independence has one-half the cross section for $p+p \rightarrow \pi^+ + d$. This gives only about 0.5 mb at 400 Mev. See R. H. Hildebrand, Phys. Rev. **89**, 1090 (1953).